MATERIALS CHEMISTRY FRONTIERS

RESEARCH ARTICLE

View Article Online
View Journal | View Issue

Cite this: *Mater. Chem. Front.*, 2025, **9**, 1421

Design of donor–acceptor covalent organic frameworks for photocatalytic hydrogen generation†

Amit Nagar,[a] Gulshan Singh,[a] Akhtar Alam,[b] Pradip Pachfule [b] and C. M. Nagaraja *[a]

The well-ordered π-conjugated backbone facilitates efficient light absorption, enhancing carrier mobility, while the tensile molecular structure allows precise tailoring of optoelectronic properties. In addition, the alternating arrangement of donor (D) and acceptor (A) segments in the well-ordered π-conjugated framework provides pathways and channels for intermolecular charge transfer (ICT). Therefore, the precise integration of the D and A moieties into the long-range ordered backbone of the COFs accelerates carrier mobilities and reduces the possibility of electron–hole recombination. COFs with a D–A system have made great progress in the related research of photocatalytic applications. It is anticipated that COFs consisting of polar hydrophilic electron-withdrawing groups (*e.g.*, COOH) can promote the efficient migration of photogenerated electrons to the Pt cocatalyst for the reduction of water protons to produce hydrogen. Herein, we demonstrate the tuning of hydrogen evolution activity by tailoring the functionality of pyrene-based COFs by introducing donor (D) and acceptor (A) functionalities to facilitate the effective charge separation through the push–pull effect. Further, in order to systematically study the photocatalytic performances, a series of D–A COFs with different linkages and electron-donating/withdrawing groups have been synthesized. This difference in photocatalytic hydrogen generation activity is further supported by different optical and electrochemical studies. This work highlights the rational tuning of the hydrogen generation activity of COFs by strategic incorporation of appropriate functionality.

Received 23rd January 2025,
Accepted 27th March 2025

DOI: 10.1039/d5qm00074b

rsc.li/frontiers-materials

Introduction

The rapid growth of the global economy has led to a massive increase in demand for fossil fuels, which in turn has been causing the rise in CO_2 levels in the atmosphere, a key factor in climate change and global warming.[1–5] It also causes other environmental problems, including biodiversity loss and accelerated climate change.[6–9] To address these issues, there is an urgent need for immediate and consistent efforts towards sustainable use of resources leading to a deteriorating dependence on fossil fuels.[10] In this scenario, hydrogen (H_2) is shown to be a promising and environmentally friendly substitute for conventional fossil fuels.[11–14] As a clean energy source, hydrogen offers the advantage of emitting no greenhouse gases during its use.[15,16] It gives more energy than hydrocarbon and there is no formation of secondary pollutants.[17,18] Hydrogen can be generated from various sources, such as fossil fuels, water, biomass, agricultural waste, and sewage sludge.[19,20] Conventional methods of producing hydrogen from fossil fuels, like coal and natural gas, are the most prevalent, expensive, and environmentally damaging, contributing the most CO_2 emissions to the atmosphere.[21] While, hydrogen production from agricultural waste and biomass is a controlled process that uses heat, steam, and oxygen without combustion.[22,23] Therefore, the production of hydrogen from water using solar-driven particulate photocatalysts is considered to be the most cost-effective and efficient method to generate hydrogen fuel with minimal environmental impact.[24–26] However, the efficiency of hydrogen generation from water in particulate photocatalytic systems is still lagging behind.[27]

Over the past decade, there has been a consistent rise in efforts focused on developing advanced photocatalysts that can convert solar energy into chemical fuels.[28,29] The progress of original photocatalysts with high efficiency and stability under working conditions remains a challenge.[30,31] As a result, several

[a] *Department of Chemistry, Indian Institute of Technology Ropar, Rupnagar 140001, Punjab, India. E-mail: cmnraja@iitrpr.ac.in; Tel: +91-1881-242229*
[b] *Department of Chemical and Biological Sciences, S. N. Bose National Centre for Basic Sciences, JD Block, Salt Lake – Sector-III, Kolkata-700 106, India*

† Electronic supplementary information (ESI) available. See DOI: https://doi.org/10.1039/d5qm00074b

countries around the world have begun to transition from a hydrocarbon-based to a hydrogen-based economy.[32] Inspired by natural photosynthesis[33] in the early 1970s, Fujishima and Honda conducted considerable research on the creation of several photocatalytic materials for the sustainable synthesis of hydrogen from water.[34] Since then, numerous metal oxide and sulfide-based semiconductor materials have been investigated as photocatalysts for hydrogen production.[35–39] In recent years, there has been growing interest in semiconductor polymers constructed from small building blocks. These materials include porous aromatic frameworks (PAFs),[40] hypercrosslinked polymers,[41] conjugated microporous polymers,[42] covalent triazine frameworks (CTFs)[43,44] and covalent organic frameworks (COFs).[45,46] Among these, COFs stand out as the most notable category of porous organic materials for various photocatalytic applications.[47]

Covalent organic frameworks are a pioneering class of porous crystalline polymers that enable precise molecular assembly into two-dimensional (2D) or three-dimensional (3D) structures through covalent bonds.[48–50] Owing to their low density,[51] large surface area,[52] high crystallinity,[53] extended π-conjugation,[54] narrow band gap[55] and flexible functionality,[56] COFs have garnered significant attention for their potential in gas adsorption/separation,[57] catalysis,[58,59] sensing,[60] optoelectronics,[61] and energy storage.[62] These properties make COFs ideal candidates for heterogeneous photocatalysis due to their ability to efficiently transport long-lived photo-excited states and high carrier mobility. Consequently, there is increasing interest in applying COFs to photocatalysis, including chemical transformations and green fuel production.[63,64] In 2014, Lotsch and colleagues were the first to report the use of a hydrazone-based COF for photocatalytic H_2 production, with platinum as a co-catalyst.[65] This breakthrough led to a surge in research into COF-based materials to develop efficient photocatalysts over the last decade. In recent years, the synthesis of COFs using a variety of building blocks, different linkages and heteronuclear molecular functionalities has been extensively explored.[66] It has been shown that the alternating arrangement of donor (D) and acceptor (A) segments in the well-ordered π-conjugated framework provides pathways and channels for intermolecular charge transfer (ICT). COFs with a D–A system facilitate efficient light absorption, enhancing carrier mobility, while the tenable molecular structure allows precise tailoring of optoelectronic properties.[67–70] It is also expected that D–A COF consists of a polar hydrophilic electron-withdrawing group (*e.g.*, COOH), which can promote the efficient migration of photogenerated electrons to Pt cocatalyst for the reduction of protons of water to produce hydrogen.

In this study, a series of pyrene-based imine-linked COFs with electron-neutral and electron-donating groups, and vinylene-linked with electron-withdrawing groups were synthesized and investigated for their potential application in photocatalytic H_2 evolution. This study revealed that strong electron-withdrawing groups on the fully conjugated backbone of COF promote the efficient migration of photogenerated electrons to the Pt cocatalyst, leading to the reduction of protons to produce hydrogen ($2H^+ + 2e^- \rightarrow H_2$). The difference in photocatalytic activity of pyrene-based COFs with different functionalities is further supported by different optical and electrochemical properties such as light harvesting, fluorescence lifetime, photocurrent, and impedance studies.

Results and discussion

The pyrene-based imine-linked COFs such as Py-Pa-H with electron-neutral and Py-Pa-CH_3 with electron-donating groups were synthesized *via* a Schiff-base condensation of 4,4′,4″,4‴-(pyrene-1,3,6,8-tetrayl) tetrabenzaldehyde (Py) with *p*-phenylenediamine (Pa) and 2,5-dimethyl-1,4-phenylenediamine (Pa-CH_3), respectively (Fig. 1a). While, Py-CN COF was prepared by following the reported procedure[71] using 4,4′,4″,4‴-(pyrene-1,3,6,8-tetrayl) tetrabenzaldehyde (Py) and 1,4-phenylenediacetonitrile (PDAN) precursors *via* Knoevenagel condensation reaction. The as-synthesized pyrene-based COFs were characterized by various analytical techniques prior to their use in photocatalytic hydrogen evolution. The phase purity and periodicity of the crystalline framework of the synthesized materials were confirmed by powder X-ray diffraction (P-XRD) analysis. The PXRD pattern revealed diffraction peaks at 3.66°, 5.28°, 7.42°, 11.20° and 23.5° of Py-Pa-H COF (Fig. 1b), and 3.64°, 5.13°, 7.23°, 11.25° and 23.4° of Py-Pa-CH_3 COF (Fig. 1c) assigned to (100), (020), (220), (330) and (001) planes, respectively. While Py-CN COF exhibited peaks at 3.63, 5.94, 7.35, and 24.70 corresponding to the (110), (210), (220), and (001) facets, respectively (Fig. 1d). Further, the material studio was used to simulate the structure of as-synthesized COFs, and it was observed that the experimental COF structure was perfectly aligned with the AA-eclipsed layer stacking model (Fig. 2e–g). The lattice parameters were confirmed through Pawley refinement in the *P*1 space group, demonstrating the matching of experimental PXRD with the simulated pattern. Detailed unit cell parameters for all three COFs are available in the ESI† (Tables S1–S3).

In the Fourier transform infrared (FT-IR) spectra of Py-PA-H/CH_3 COFs, the appearance of a new band around 1620 cm^{-1} corresponding to C=N stretching and disappearance of free C=O (1698 cm^{-1}) stretching band of 4,4′,4″,4‴-(pyrene-1,3,6,8-tetra) tetra benzaldehyde and NH_2 stretching frequency of p-phenylenediamine (3372 cm^{-1}), and 2,5-dimethyl-1,4-phenylenediamine (3399 cm^{-1}) suggest the formation of Py-PA-H/CH_3 COFs (Fig. 2a and b). Whereas, in the FT-IR spectra of Py-CN COF, the –C=O– stretching frequency of starting aldehyde monomers at 1698 cm^{-1} disappeared and a new band at 1665 cm^{-1} attributed to –C=C– stretching appeared indicating complete conversion of the building blocks. Additionally, the shift of the nitrile (–C≡N) vibration band from 2249 cm^{-1} in the PDAN monomer to 2210 cm^{-1} in the Py-CN COF indicates the successful formation of the cyanovinylene (C=C–CN) linkage (Fig. 2c).

The solid-state ^{13}C cross-polarization/magic angle spinning (CP/MAS) nuclear magnetic resonance (NMR) spectroscopy

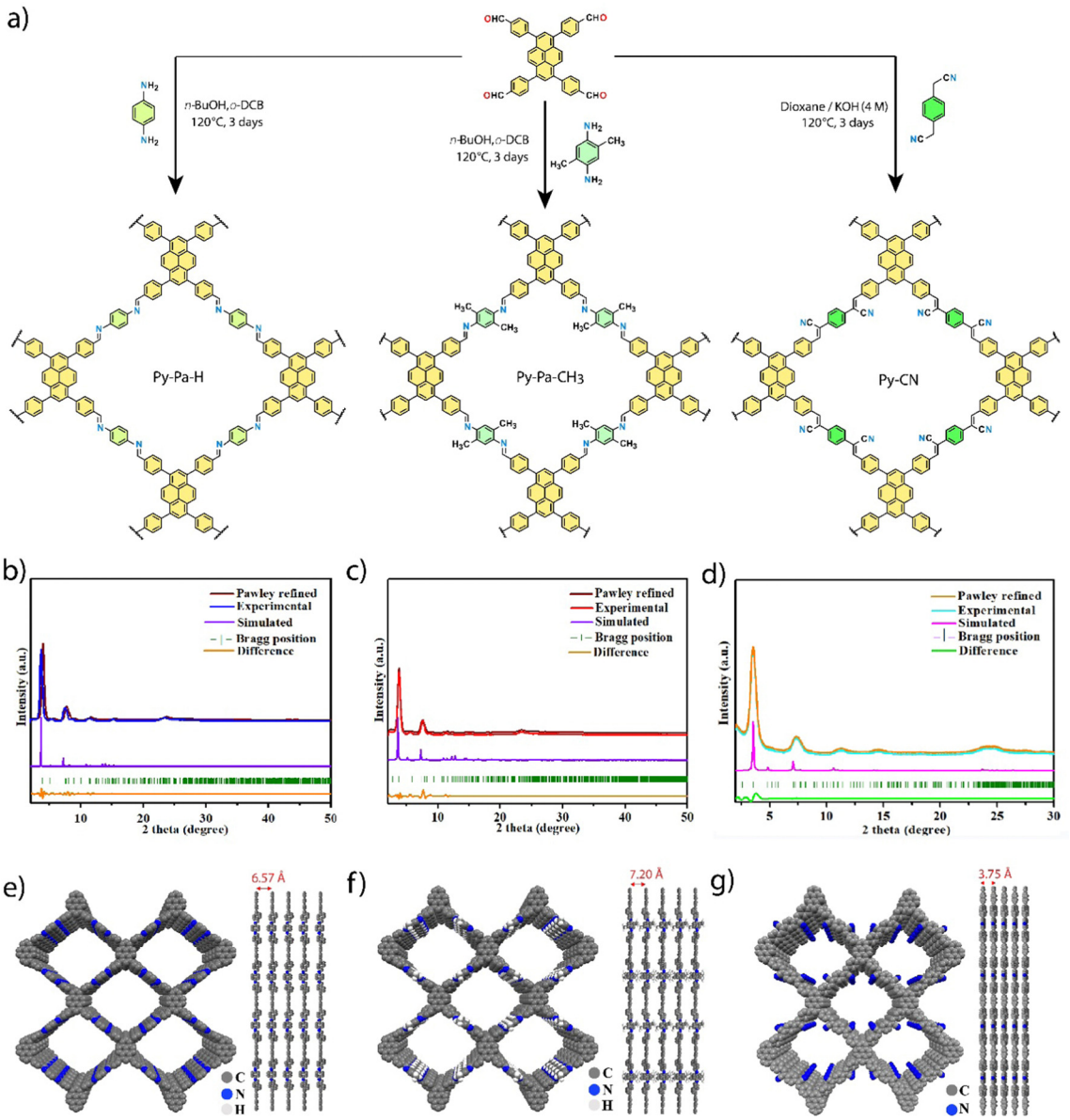

Fig. 1 Synthesis of pyrene-based donor–acceptor COFs. (a) Scheme of the synthesis of Py-Pa-H, Py-Pa-CH_3 and Py-CN COFs. Comparison of simulated and experimental PXRD patterns for (b) Py-Pa-H, (c) Py-Pa-CH_3, and (d) Py-CN COFs. The ideal AA eclipsed (AA) stacking mode for (e) Py-Pa-H, (f) Py-Pa-CH_3, and (g) Py-CN COFs.

analyses of the synthesized COFs confirmed the complete conversion of the monomers, as no residual carbonyl resonance was located at ~190 ppm (Fig. 2d–f). Py-Pa-H/CH_3 COFs showed the imine (–C═N) carbon resonance around 160 ppm, while the Py-Pa-CH_3 COF showed an additional carbon peak at 13 ppm for the –CH_3 group. The successful formation of the desired Py-CN COF was further confirmed by the appearance of a carbon resonance signal corresponding to the cyanide group (–CN) at 105 ppm, along with a resonance at 140 ppm attributed to the –C═C– linkage.

The permanent porosity of Py-Pa-H, Py-Pa-CH_3, and Py-CN COF was determined through nitrogen adsorption–desorption analysis at 77 K. Before the measurements, the as-prepared samples were activated at 120 °C under vacuum for 12 hours. The resulting adsorption curves exhibited a type-II isotherm. The Brunauer–Emmett–Teller (BET) surface areas of the COFs were calculated to be 2273 $m^2 g^{-1}$, 1883 $m^2 g^{-1}$ and 620 $m^2 g^{-1}$ for Py-Pa-H, Py-Pa-CH_3 and Py-CN COFs, respectively (Fig. 2g–i). The pore size distribution (PSD) analysis reveals that Py-Pa-H, Py-Pa-CH_3 and Py-CN COFs possess pore sizes of approximately 2.4 nm, 2.1 and 2.0 nm, respectively (Fig. S2a–S2c, ESI†). The morphology of the COFs was examined by field-emission scanning electron microscopy and high-resolution transmission electron microscopy. Py-Pa-H, Py-Pa-CH_3 and Py-CN COFs showed rod-like morphology (Fig. S3a–S3f, ESI†). Thermogravimetric analyses (TGA) were performed to assess the thermal stability of the COFs. The TGA plots of Py-Pa-H, Py-Pa-CH_3, and Py-CN COFs showed good thermal stability (Fig. S4a–S4c, ESI†).

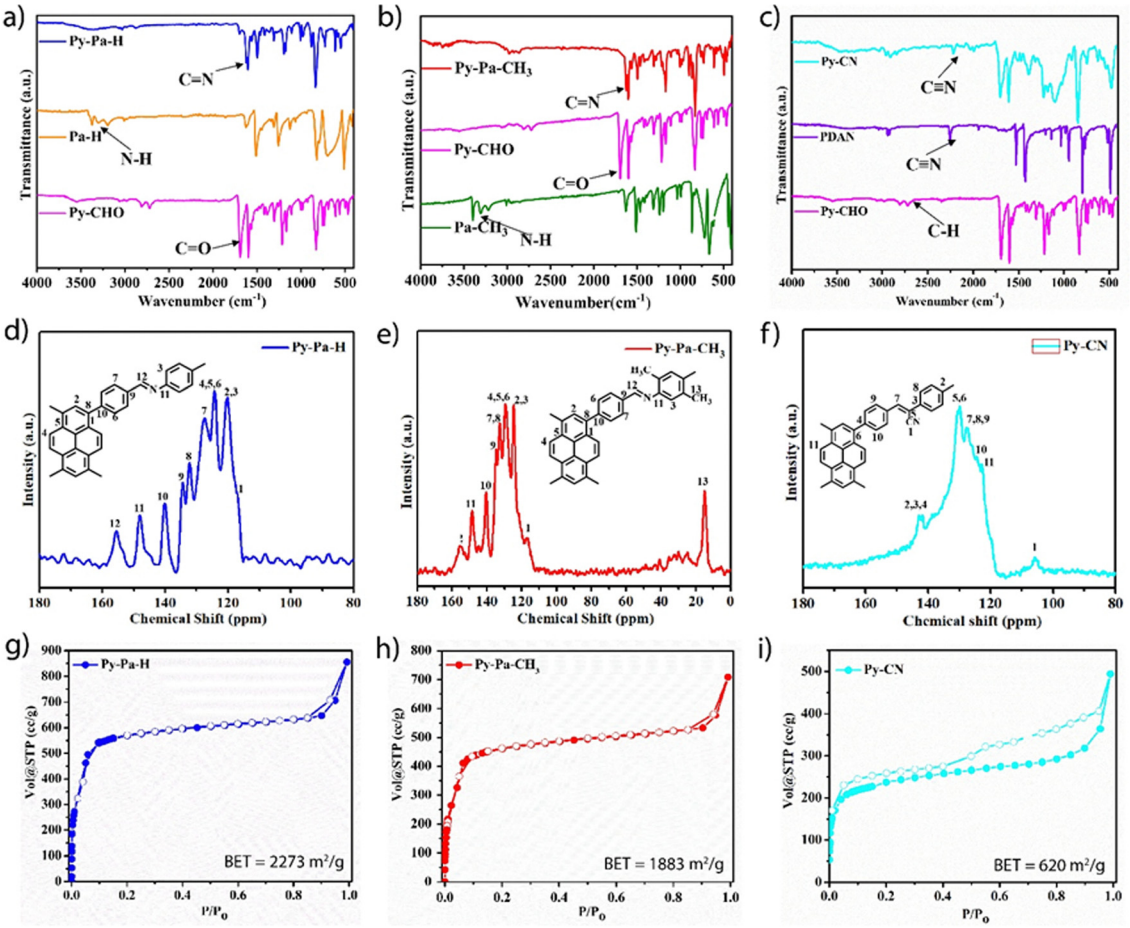

Fig. 2 Characterization of pyrene-based donor–acceptor COFs. FT-IR spectra of (a) Py-Pa-H, (b) Py-Pa-CH_3, and (c) Py-CN COFs with their corresponding precursors. Solid-state ^{13}C CP-MAS NMR spectra of (d) Py-Pa-H, (e) Py-Pa-CH_3, and (f) Py-CN COFs. N_2 adsorption (solid symbols) and desorption (open symbols) isotherms of (g) Py-Pa-H, (h) Py-Pa-CH_3, and (i) Py-CN COFs conducted at 77 K.

The optical properties of the COFs were assessed using ultraviolet-visible spectroscopy diffuse reflectance spectroscopy (DRS). The as-synthesized Py-Pa-H, Py-Pa-CH_3 and Py-CN COFs exhibited a broad absorption range within the visible light spectrum (Fig. 3a). Notably, Py-CN COF displayed a noticeable red shift in the absorption in comparison to Py-Pa-H and Py-Pa-CH_3 COFs, indicating a higher degree of conjugation in Py-CN COF. The absorption band edges for Py-Pa-CH_3, Py-Pa-H, and Py-CN COFs are 530, 560, and 590 nm, respectively. Tauc plot analysis determined the optical band gaps to be 2.13 eV for Py-CN, 2.27 eV for Py-Pa-H, and 2.37 eV for Py-Pa-CH_3 COFs, (Fig. 3b), which are suitable for photocatalytic water splitting. Additionally, valence band (VB) energy determined from VB-XPS analysis is 1.12 eV for Py-Pa-H, 1.58 eV for Py-Pa-CH_3, and

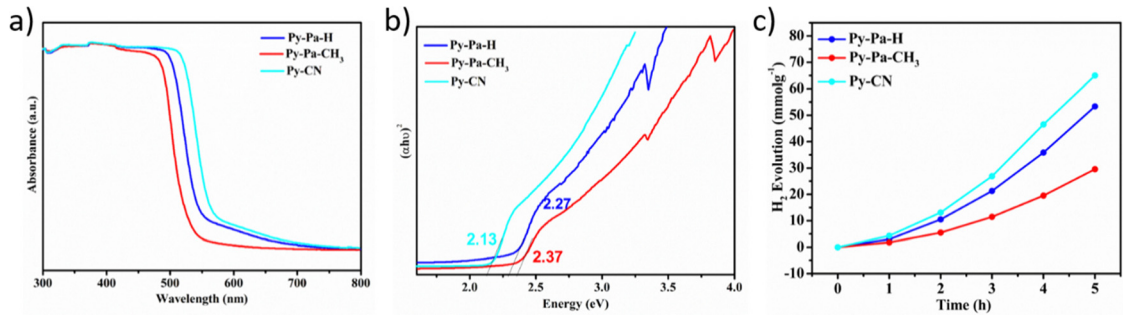

Fig. 3 Photophysical properties of pyrene-based donor–acceptor COFs. (a) UV-vis DRS spectra of Py-Pa-H, Py-Pa-CH_3 and Py-CN COFs. (b) The corresponding Tauc plots of Py-Pa-H, Py-Pa-CH_3 and Py-CN COFs. (c) Photocatalytic H_2 evolution by Py-Pa-H, Py-Pa-CH_3 and Py-Pa-CN COFs over 3 wt% Pt-deposited with ascorbic acid (0.1 M) in water under visible light ($\lambda \geq 420$ nm).

0.84 eV for Py-CN COF (Fig. S5a, ESI†). Using the Tauc plot and VB-XPS data, the conduction band edge positions were calculated and are presented in Fig. S5b (ESI†).

Photocatalytic activity

Following the confirmation of the structures of the COFs and their photophysical properties, photocatalytic performance was examined for hydrogen evolution from water. The typical experiments were conducted in a Pyrex glass reactor, using an aqueous solution containing in situ-generated Pt nanoparticles as a cocatalyst and ascorbic acid as a sacrificial electron donor (SED) under visible-light ($\lambda \geq 420$ nm) irradiation. Control tests showed that no hydrogen was produced without the presence of light or the photocatalyst. Only minimal hydrogen evolution (14 μmol g^{-1} h^{-1}) was observed without Pt cocatalyst employing Py-CN COF. For the photocatalytic hydrogen evolution tests, 3.5 mg of the COF as catalyst was added to 30 mL of water containing 0.1 M ascorbic acid and 3 wt% of Pt, and the system was irradiated with visible light at 25 °C. All COFs were tested under the same conditions to ensure an accurate comparison of their efficiencies. The results showed that Py-CN COF exhibited the highest hydrogen evolution rate (HER) of 13.0 mmol g^{-1} h^{-1}, compared to Py-Pa-H (10.7 mmol g^{-1} h^{-1}), and Py-Pa-CH_3 (5.7 mmol g^{-1} h^{-1}) (Fig. 3c). The higher HER of Py-CN was ascribed to the stronger absorption of visible light, narrow band gap, and the presence of strong cyanovinylene linkage in the COF backbone. Since the electron-withdrawing –CN group plays a crucial role in the photocatalytic activity towards hydrogen evolution. Further, we were interested in introducing a polar hydrophilic electron-withdrawing carboxylic acid (–COOH) group into the COF framework, which can promote efficient migration of photogenerated electrons to the Pt cocatalyst for the reduction of water protons to produce hydrogen. Therefore, we synthesized a pyrene-based carboxylic acid functionalized D–A COF (Py-COOH) by post-synthetic modification of Py-CN COF using aqueous NaOH (10 M) and ethanol (1/1, v/v) mixture at 90 °C for 3 days (Fig. 4a). The Py-COOH COF was fully characterized prior to the photocatalytic experiments. In FT-IR spectra of Py-COOH COF, the disappearance of the nitrile (C≡N) stretching frequency (2249 cm^{-1}) and the appearance of new bands at 1670 cm^{-1} and 1400 cm^{-1}, corresponding to the C=O stretching frequency of –COOH group, suggest the conversion of –CN into –COOH group (Fig. 4b). The solid-state ^{13}C CP/MAS NMR spectrum of Py-COOH COF showed the appearance of carbon resonance at 174.7 ppm, corresponding to the –COOH group (Fig. 4c). Notably, the absence of the carbon resonance corresponding to the cyanide group at 105.6 ppm further confirms the complete conversion of –CN to –COOH group.

In the PXRD pattern of Py-COOH COF, the low-angle peak at $2\theta = 3.69°$ (110 facets) indicates the crystalline structure of the material (Fig. 4d). Additional peaks were observed at 2θ values of 5.1°, 7.4°, 11.3°, 14.6°, and 24.3°, corresponding to the (210), (220), (240), (520), and (001) planes, respectively. The peak at 24.3° is associated with π–π stacking between the layers of Py-COOH COF. It is noteworthy that the experimental PXRD spectrum closely matches the simulated PXRD pattern. The most likely 2D model of the Py-COOH COF was also optimized using an eclipsed stacking model in the *P*1 space group (Fig. 4e and Table S4, ESI†), which closely matches the experimental PXRD pattern. However, a lower surface area of the Py-COOH COF (599 m^2 g^{-1}) compared to Py-CN COF could be attributed

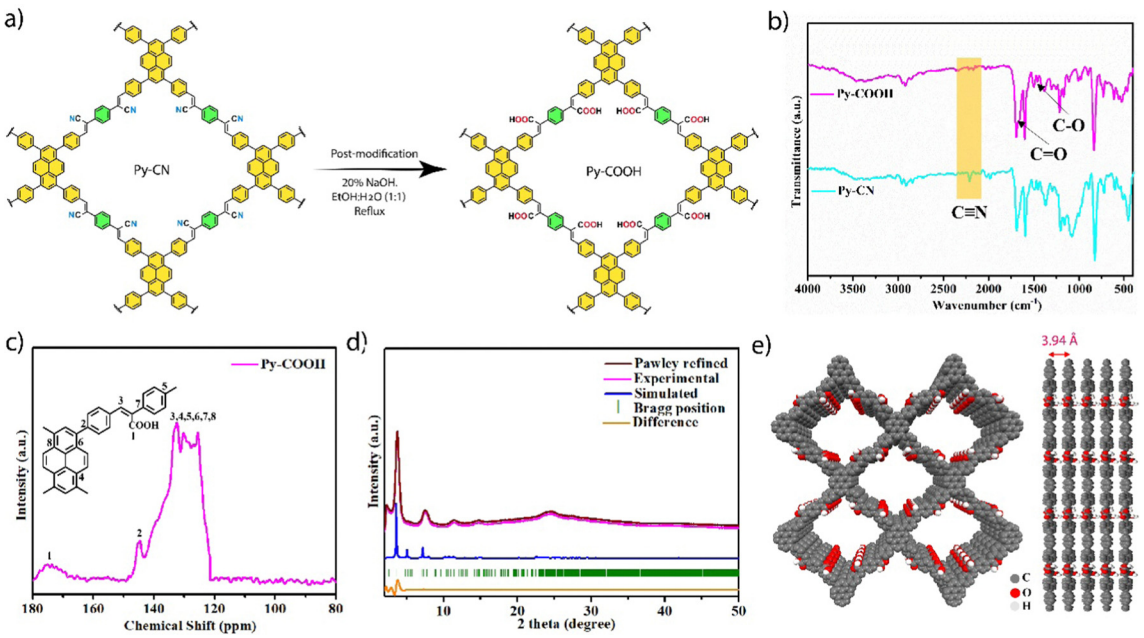

Fig. 4 Synthesis and characterization of pyrene-based donor–acceptor COF. (a) Scheme of the synthesis of carboxylic acid functionalized COF (Py-COOH). (b) FT-IR spectra of Py-COOH COF in comparison with Py-CN COF. (c) Solid-state ^{13}C CP-MAS NMR spectrum of Py-COOH COF. (d) Comparison of simulated and experimental PXRD patterns for Py-COOH COF. (e) The ideal AA eclipsed (AA) stacking mode for Py-COOH COF.

to the presence of bigger-sized carboxylic groups[72] (Fig. S6a, ESI†).

Furthermore, XPS analyses were performed to examine the chemical composition of the COFs. The XPS survey scans confirmed the presence of constituent elements (C, O) in Py-COOH and (C, N) in Py-CN and Py-Pa-H/CH_3 COFs (Fig. S7a, ESI†). The C 1s spectra of Py-COOH showed three C binding energies at 284.4 eV, 284.9 eV, and 285.9 eV, corresponding to C═C, C–C–OH, and C═O bonds, respectively (Fig. S7b, ESI†). The O 1s spectra show two binding energy peaks at 531.6 eV and 532.7 eV, corresponding to –C═O and ═C–OH groups (Fig. S7c, ESI†). The Py-COOH COF exhibited a well-defined fiber-like morphology (Fig. S8a and S8b, ESI†) and EDX elemental mapping showed the presence of constitute elements (C, and O) uniformly distributed on the frameworks (Fig. S8c, ESI†). To evaluate the chemical stability of Py-COOH COF, 10 mg of the material was immersed in various solvents, including acetone, methanol, THF, 1 M HCl, and 1 M NaOH, for three days. After filtration and drying, PXRD analysis showed no shift in peak positions, confirming that the crystallinity was preserved, as demonstrated in (Fig. S9, ESI†). It is interesting to note that the Py-COOH COF with a narrower band gap of 2.04 eV shows a redder shift in absorption compared to the Py-CN COF with a band gap of 2.13 eV (Fig. S10, ESI†). Additionally, valence band (VB) energy determined from XPS is 0.68 eV for Py-Pa-H and 0.84 eV for Py-CN COF (Fig. S10c, ESI†). Using the Tauc plot and VB-XPS data, the conduction band energy was calculated and is presented in (Fig. S10d, ESI†).

Considering these promising properties, Py-COOH COF was used for the photocatalytic H_2 generation experiment, which showed a hydrogen evolution rate of 18.8 mmol g^{-1} h^{-1}, which is 1.45 times higher than that of Py-CN COF (Fig. 5a and Table S5, ESI†). It was observed that the Pt loading had a significant effect on the catalyst's performance and the optimum HER was achieved with 3 wt% Pt loading, while higher loading (8 wt%) led to agglomeration on the COF surface, thereby reducing hydrogen production (Fig. 5b).[73] Notably, hydrogen evolution activity performed under basic conditions using Triethanolamine (TEOA) as SED revealed no activity by imine-based COFs (Py-Pa-H and Py-Pa-CH_3).[74] However, the vinylene-based COF (Py-CN and Py-COOH) showed an H_2 generation rate of 798 μmol g^{-1} h^{-1} and 1287 μmol g^{-1} h^{-1} which is significantly lower in comparison to the HER observed in acidic conditions with ascorbic acid as SED. Further, a comparison of the hydrogen evolution performance with literature-reported COFs unveiled the superior performance of Py-COOH

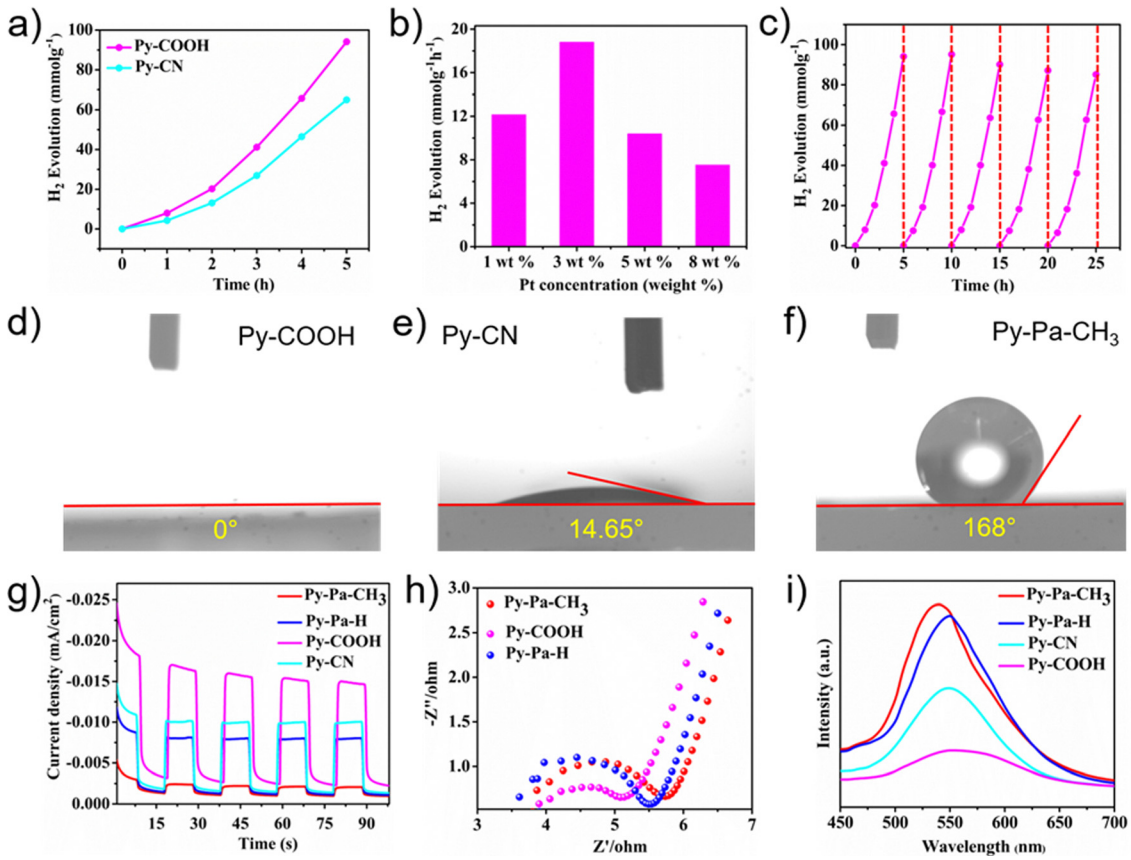

Fig. 5 (a) Photocatalytic H_2 evolution of Py-COOH and Py-CN COFs. (b) H_2 evolution at different platinum concentrations. (c) Photostability for H_2 generation of Py-COOH COF tested over 25 h with evacuation every 5 h. The water contact angle of (d) Py-COOH (e) Py-CN and (f) Py-Pa-CH_3 COFs. (g) Photocurrent response of Py-Pa-H, Py-Pa-CH_3, Py-CN and Py-COOH COFs (g) EIS Nyquist plots of Py-Pa-H, Py-Pa-CH_3 and Py-COOH COFs (i) Photoluminescence (PL) spectra of Py-Pa-H, Py-Pa-CH_3, Py-CN and Py-COOH COFs with the excitation wavelength of 400 nm.

COF (Table S6, ESI†). To evaluate the robustness of the Py-COOH COF, a recycling test was performed, demonstrating the excellent photocatalytic stability of the Py-COOH COF, as there was only a slight decline in hydrogen generation activity after five cycles (Fig. 5c).

The superior photocatalytic activity of the Py-COOH COF is attributed to the presence of the polar hydrophilic electron-withdrawing COOH group, which promoted the efficient migration of photogenerated electrons to Pt cocatalyst for the reduction of protons of water to generate hydrogen. A contact angle test was conducted to assess the hydrophilicity of the COFs and validate the results. Py-COOH COF showed high hydrophilicity with immediate water permeation compared to the other COFs (Fig. 5d–f and Fig. S11, ESI†). In addition, electrochemical impedance spectroscopy (EIS), transient photocurrent response (TPR), and photoluminescence (PL) were performed to gain a more detailed understanding of the separation and migration of photogenerated electron–hole pairs in these COF materials. Further, the Py-COOH COF exhibited a greater photocurrent response compared to the Py-CN and Py-Pa-H/CH_3 COFs, indicating a more efficient separation of photoinduced electron–hole pairs (Fig. 5g). Besides, Py-COOH COF showed a comparatively smaller semicircle radius, suggesting that the electron-withdrawing functional groups reduce the resistance to interfacial charge transfer (Fig. 5h). Whereas, the PL spectra revealed that Py-COOH COF has the lowest PL intensity, indicating its superior ability to suppress electron–hole recombination (Fig. 5i). Furthermore, photoluminescence decay measurements demonstrated that Py-COOH has a significantly longer radiative lifetime (2.1 ns) compared to Py-Pa-H (1.78 ns), Py-CN (1.99 ns) and Py-Pa-CH_3 (1.7 ns), suggesting a higher probability of photogenerated charges participating in the photocatalytic process (Fig. S12, ESI†).

To further evaluate the stability of the recycled catalyst, several characterization techniques such as PXRD (Fig. S13a, ESI†), FT-IR (Fig. S13b, ESI†), and FE-SEM (Fig. S13d, ESI†) were assessed, which closely matched those of the fresh material, confirming that the structure of the Py-COOH COF remained largely unchanged. However, after the photocatalytic process, Py-COOH COF became covered with discrete Pt nanoparticles (2–3 nm in size) moulded *in situ*, as confirmed by HR-TEM analysis (Fig. S14, ESI†).

Photocatalysis mechanism of hydrogen generation

The results indicate that Py-COOH COF outperforms Py-Pa-H, Py-Pa-CH_3, and Py-CN COFs in photocatalytic hydrogen evolution. This higher efficiency is due to the structure–function relationship of the Py-COOH COF, which possesses the electron donor (pyrene) and acceptor (COOH) units. This results in an optimal band gap, strong light absorption in the UV-visible range, abundant water docking sites, and efficient separation of the photo-excited electrons and holes. Upon exposure to visible light, the COF absorbs energy and electrons are excited from the valence band (VB) to the conduction band (CB), leaving holes behind. The excited electrons then move to the platinum (Pt) surface, which acts as a cocatalyst to reduce water to hydrogen. A sacrificial agent is used to trap the holes and suppress the recombination of the electrons and holes, making the reduction of water more effective. In this work, Py-COOH COF has more active sites for water reduction due to the presence of the hydrophilic carboxyl group (–COOH). The –COOH group also stabilizes the Pt cocatalyst,[59] facilitating faster and smoother electron transfer to the cocatalyst's surface. At the same time, the sacrificial agent (ascorbic acid) captures the generated holes, completing the photocatalytic reaction. The increased hydrophilicity of Py-COOH also improves its interaction with water, helping the cocatalyst to more efficiently reduce water to hydrogen, speeding up the entire process compared to the other Py-Pa-H/CH_3, Py-CN COFs (Fig. 6).

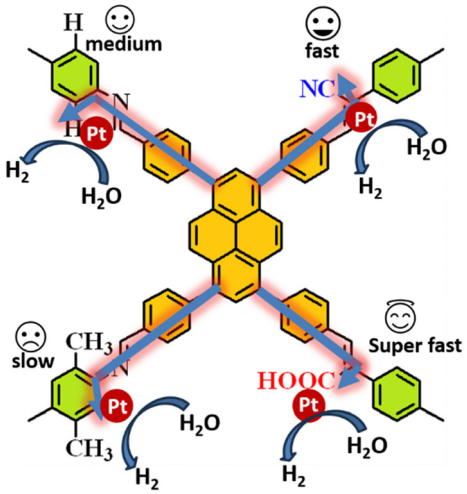

Fig. 6 The proposed mechanism for photocatalytic hydrogen production with a comparison of Py-Pa-H, Py-Pa-CH_3, Py-CN and Py-COOH COF.

Conclusions

In conclusion, we have prepared crystalline two-dimensional donor–acceptor covalent organic framework (Py-COOH) decorated with a polar hydrophilic electron-withdrawing –COOH group. The conjugated vinylene-linked Py-COOH COF exhibits suitable band gap and conduction band position, which enhance the visible light absorption, prolong the excited state lifetime, and provide active sites for easy photodeposition of platinum nanoparticles acting as cocatalysts. Therefore, the strong electron-accepting moiety (COOH) contributes to the superior photocatalytic performance of Py-COOH COF with a HER of 18.8 mmol g^{-1} h^{-1} compared to Py-CN COF (13.0 mmol g^{-1} h^{-1}) and the isostructural Py-Pa-H (10.7 mmol g^{-1} h^{-1}) and Py-Pa-CH_3 COFs (5.7 mmol g^{-1} h^{-1}), which lack a donor–acceptor system—highlighting the importance of band engineering in photocatalysis. In addition, the Py-COOH COF remains highly stable even after multiple photocatalytic cycles—a promising approach to advance solar-driven

hydrogen production using durable, reusable COF-based photocatalysts.

Data availability

Data will be available on request.

Conflicts of interest

The authors declare no conflict of interest.

Acknowledgements

C. M. N. acknowledges SERB (CRG/2022/006762) and CSIR (01/3131/23/EMR-II) for financial support. AN thanks CSIR (file No. 09/1005(0044)/2020-EMR-I) for funding. The authors acknowledge the Institute NMR Facility, IISc Bangalore, for solid-state cross-polarization/magic angle spinning (CP/MAS) nuclear magnetic resonance (NMR) spectroscopy. P. P. acknowledges the financial support from the S. N. Bose National Centre for Basic Sciences, the Technical Research Centre (TRC), and the Department of Science and Technology (SRG/2022/000217).

References

1 R. Cassia, M. Nocioni, N. C. Aragunde and L. Lamattina, Climate Change and the Impact of Greenhouse Gasses: CO_2 and NO, Friends and Foes of Plant Oxidative Stress, *Front. Plant Sci.*, 2018, **9**, 473.

2 N. S. Lewis and D. G. Nocera, Powering the planet: chemical challenges in solar energy utilization, *Proc. Natl. Acad. Sci. U. S. A.*, 2006, **103**, 15729–15735.

3 S. Dhingra, M. Sharma, V. Krishnan and C. M. Nagaraja, Design of noble metal-free $CoTiO_3/Zn_{0.5}Cd_{0.5}S$ heterostructure photocatalyst for selective synthesis of furfuraldehyde combined with H_2 production, *J. Colloid Interface Sci.*, 2022, **608**, 1040–1050.

4 D. Shindell and C. J. Smith, Climate and air-quality benefits of a realistic phase-out of fossil fuels, *Nature*, 2019, **573**, 408–411.

5 K. Prakash, B. Mishra, D. D. Dıaz, C. M. Nagaraja and P. Pachfule, Strategic design of covalent organic frameworks (COFs) for photocatalytic hydrogen generation, *J. Mater. Chem. A*, 2023, **11**, 14489–14538.

6 A. E. H. Berjawi, S. L. Walker, C. Patsios and S. H. R. Hosseini, An evaluation framework for future integrated energy systems: A whole energy systems approach, *Renewable Sustainable Energy Rev.*, 2021, **145**, 111163.

7 K. H. Ng, S. Y. Lai, C. K. Cheng, Y. W. Cheng and C. C. Chong, Photocatalytic water splitting for solving energy crisis: Myth, Fact or Busted?, *Chem. Eng. J.*, 2021, **417**, 128847.

8 T. Simon, N. Bouchonville, M. J. Berr, A. Vaneski, A. Adrović, D. Volbers, R. Wyrwich, M. Döblinger, A. S. Susha, A. L. Rogach, F. Jäckel, J. K. Stolarczyk and J. Feldmann, Redox shuttle mechanism enhances photocatalytic H_2 generation on Ni-decorated CdS nanorods, *Nat. Mater.*, 2014, **13**, 1013–1018.

9 Z. Wang, C. Li and K. Domen, Recent developments in heterogeneous photocatalysts for solar-driven overall water splitting, *Chem. Soc. Rev.*, 2019, **48**, 2109–2125.

10 W. Zhou, J. Jia, J. Lu, L. Yang, D. Hou and G. Li, Solar-Driven Hydrogen Production: Recent Advances, Challenges, and Future Perspectives, *Nano Energy*, 2016, **28**, 29–43.

11 P. J. Megía, A. J. Vizcaíno, J. A. Calles and A. Carrero, Hydrogen Production Technologies: From Fossil Fuels toward Renewable Sources. A Mini Review, *Energy Fuels*, 2021, **35**, 16403–16415.

12 W. Chen, L. Wang, D. Mo, F. He, Z. Wen, X. Wu, H. Xu and L. Chen, Strong-Base-Assisted Synthesis of a Crystalline Covalent Triazine Framework with High Hydrophilicity *via* Benzylamine Monomer for Photocatalytic Water Splitting, *Angew. Chem., Int. Ed.*, 2020, **59**, 16902–16909.

13 H. Tong, S. Ouyang, Y. Bi, N. Umezawa, M. Oshikiri and J. Ye, Nano-photocatalytic Materials: Possibilities and Challenges, *Adv. Mater.*, 2011, **24**, 229–251.

14 S. Ghosh, H. Küçükkeçeci, R. P. Paitandi, V. Weigelt, V. Dippold, S. Seki and A. Thomas, Low band gap semiconducting covalent organic framework films with enhanced photocatalytic hydrogen evolution, *J. Mater. Chem. A*, 2024, **12**, 247–255.

15 A. K. Singh, A. Jaryal, S. K. Patel, D. Kumar, E. S. S. Iyer, K. Kailasam and A. Indra, Deciphering ligand-controlled charge transfer from a metal-organic framework to cadmium sulfide for enhanced photocatalytic hydrogen evolution reaction, *J. Mater. Chem. A*, 2023, **11**, 16724–16733.

16 S. A. Ali, S. Majumdar, P. K. Chowdhury, M. S. Alshehri and T. Ahmad, Ultrafast Charge Transfer Dynamics in Multifaceted Quaternary Te-$MoTe_2$-MoS_2/ZnO S-Scheme Heterostructured Nanocatalysts for Efficient Green Hydrogen Energy, *ACS Appl. Energy Mater.*, 2024, **7**, 7325–7337.

17 J. Ran, J. Qu, H. Zhang, T. Wen, H. Wang, S. Chen, L. Song, X. Zhang, L. Jing, R. Zheng and S.-Z. Qiao, 2D Metal-Organic Framework Nanosheet: A Universal Platform Promoting Highly Efficient Visible-Light-Induced Hydrogen Production, *Adv. Energy Mater.*, 2019, **9**, 1803402.

18 Z. Abdin, A. Zafaranloo, A. Rafiee, W. Mérida, W. Lipiński and K. R. Khalilpour, Hydrogen as an Energy Vector, *Renewable Sustainable Energy Rev.*, 2020, **120**, 109620.

19 W. Liu, Y. Cui, X. Du, Z. Zhang, Z. Chao and Y. Deng, High-efficiency hydrogen evolution from native biomass electrolysis, *Energy Environ. Sci.*, 2016, **9**, 467–472.

20 A. Alnouss, G. McKay and T. Al-Ansari, Enhancing waste to hydrogen production through biomass feedstock blending: A techno-economic-environmental evaluation, *Appl. Energy*, 2020, **266**, 144885.

21 M. Watanabe, H. Inomata and K. Arai, Catalytic hydrogen generation from biomass (glucose and cellulose) with ZrO_2 in supercritical water, *Biomass Bioenergy*, 2021, **22**, 405–410.

22 J. Qi, W. Zhang and R. Cao, Solar-to-Hydrogen Energy Conversion Based on Water Splitting, *Adv. Energy Mater.*, 2018, **8**, 1701620.
23 J. V. Karaeva, Hydrogen production at centralised utilization of agricultural waste, *Int. J. Hydrogen Energy*, 2021, **46**, 34089–34096.
24 A. Fujishima, T. N. Rao and D. A. Tryk, Titanium dioxide photocatalysis, *J. Photochem. Photobiol., C*, 2000, **1**, 1–21.
25 Y.-J. Yuan, Z.-T. Yu, D.-Q. Chen and Z.-G. Zou, Metal-complex chromophores for solar hydrogen generation, *Chem. Soc. Rev.*, 2017, **46**, 603–631.
26 Y. Wang, A. Vogel, M. Sachs, R. S. Sprick, L. Wilbraham, S. J. A. Moniz, R. Godin, M. A. Zwijnenburg, J. R. Durrant, A. I. Cooper and J. Tang, Current understanding and challenges of solar-driven hydrogen generation using polymeric photocatalysts, *Nat. Energy*, 2019, **4**, 746–760.
27 Q. Wang, T. Hisatomi, Q. Jia, H. Tokudome, M. Zhong, C. Wang, Z. Pan, T. Takata, M. Nakabayashi, N. Shibata, Y. Li, I. D. Sharp, A. Kudo, T. Yamada and K. Domen, Scalable water splitting on particulate photocatalyst sheets with a solar-to-hydrogen energy conversion efficiency exceeding 1%, *Nat. Mater.*, 2016, **15**, 611–615.
28 A. Galushchinskiy, R. G. Gómez, K. McCarthy, P. Farràs and A. Savateev, Progress in Development of Photocatalytic Processes for Synthesis of Fuels and Organic Compounds under Outdoor Solar Light, *Energy Fuels*, 2022, **36**, 4625–4639.
29 H. Tong, S. Ouyang, Y. Bi, N. Umezawa, M. Oshikiri and J. Ye, Nano-photocatalytic Materials: Possibilities and Challenges, *Adv. Mater.*, 2012, **24**, 229–251.
30 H. Wang, L. Zhang, Z. Chen, J. Hu, S. Li, Z. Wang, J. Liu and X. Wang, Semiconductor heterojunction photocatalysts: design, construction, and photocatalytic performances, *Chem. Soc. Rev.*, 2014, **43**, 5234–5244.
31 H. Khan, S. E. Lofland, K. V. Ramanujachary, N. Alhokbany and T. Ahmad, *ACS Appl. Energy Mater.*, 2023, **6**, 8102–8110.
32 R. Agarwal, Transition to a Hydrogen-Based Economy: Possibilities and Challenges, *Sustainability*, 2022, **14**, 15975.
33 N. Xu, Y. Diao, Z. Xu, H. Ke and X. Zhu, Covalent Triazine Frameworks Embedded with Ir Complexes for Enhanced Photocatalytic Hydrogen Evolution, *ACS Appl. Energy Mater.*, 2022, **5**, 7473–7478.
34 A. Fujishima and K. Honda, Electrochemical Photolysis of Water at a Semiconductor Electrode, *Nature*, 1972, **238**, 37–38.
35 N. Cheng, S. Stambula, D. Wang, M. N. Banis, J. Liu, A. Riese, B. Xiao, R. Li, T.-K. Sham, L.-M. Liu, G. A. Botton and X. Sun, Platinum single-atom and cluster catalysis of the hydrogen evolution reaction, *Nat. Commun.*, 2016, **7**, 13638.
36 M. Kaur and C. M. Nagaraja, Template-free Synthesis of Zn1-xCdxS Nanocrystals with Tunable Band Structure for Efficient Water Splitting and Reduction of Nitroaromatics in Water, *ACS Sustainable Chem. Eng.*, 2017, **5**, 4293–4303.
37 Y. P. Xie, G. S. Wang, E. L. Zhang and X. Zhang, *Chin. J. Inorg. Chem.*, 2017, **33**, 177–209.
38 S. Dhingra, T. Chhabra, V. Krishnan and C. M. Nagaraja, Visible-light-driven selective oxidation of biomass-derived HMF to DFF coupled with H_2 generation by noble metal-free $Zn_{0.5}Cd_{0.5}S/MnO_2$ heterostructures, *ACS Appl. Energy Mater.*, 2020, **3**, 7138–7148.
39 B. Debnath, S. Dhingra and C. M. Nagaraja, Recent developments in the design of CdxZn1-xS based photocatalysts for sustainable production of hydrogen, *Sol. RRL.*, 2021, **5**, 2100226.
40 Y. Yuan and G. Zhu, Porous Aromatic Frameworks as a Platform for Multifunctional Applications, *ACS Cent. Sci.*, 2019, **5**, 409–418.
41 L. Tan and B. Tan, Hypercrosslinked porous polymer materials: design, synthesis, and applications, *Chem. Soc. Rev.*, 2017, **46**, 3322–3356.
42 G. Singh, N. Duhan, T. J. D. Kumar and C. M. Nagaraja, Pyrene-Based Nanoporous Covalent Organic Framework for Carboxylation of C-H Bonds with CO_2 and Value-Added 2-Oxazolidinones Synthesis under Ambient Conditions, *ACS Appl. Mater. Interfaces*, 2024, **16**, 5857–5868.
43 R. Kishan, P. Rani, G. Singh and C. M. Nagaraja, Functionalized Covalent Triazine Framework (CTF) for Catalytic CO_2 Fixation and Synthesis of Value-Added Chemicals, *Cryst. Growth Des.*, 2024, **24**, 7878–7887.
44 J. Roeser, K. Kailasam and A. Thomas, Covalent Triazine Frameworks as Heterogeneous Catalysts for the Synthesis of Cyclic and Linear Carbonates from Carbon Dioxide and Epoxides, *ChemSusChem*, 2012, **5**, 1793–1799.
45 A. P. Côté, A. I. Benin, N. W. Ockwig, M. O'Keeffe, A. J. Matzger and O. M. Yaghi, Porous, Crystalline, Covalent Organic Frameworks, *Science*, 2005, **310**, 1166–1170.
46 S. Kandambeth, K. Dey and R. Banerjee, Covalent Organic Frameworks: Chemistry beyond the Structure, *J. Am. Chem. Soc.*, 2019, **141**, 1807–1822.
47 Y. Yang, S. Peng, S. Chen, F. Kang, J. Fan, H. Zhang, X. Yu, J. Li and Q. Zhang, Pyrene-based covalent organic frameworks (PyCOFs): a review, *Nanoscale Horiz.*, 2024, **9**, 2198–2233.
48 S. Dutta, J. I. H. García, B. Mishra, D. D. Díaz and P. Pachfule, Synthesis and Applications of Cage-Based Covalent Organic Frameworks, *Cryst. Growth Des.*, 2024, **24**, 6081–6094.
49 V. Parihar, G. Singh, N. Duhan, S. Kumar, T. J. D. Kumar and C. M. Nagaraja, Non-Noble Metal Anchored 2D Covalent Organic Framework for Ambient CO_2 Fixation to High-Value Compounds, *ChemSusChem*, 2025, **18**, e202401497.
50 R.-R. Liang, R.-H. A, S.-Q. Xu, Q.-Y. Qi and X. Zhao, Fabricating Organic Nanotubes through Selective Disassembly of Two-Dimensional Covalent Organic Frameworks, *J. Am. Chem. Soc.*, 2020, **142**, 70–74.
51 V. Swaroopa, D. Devulapalli, R. Kushwaha, E. Ovalle, H. D. Singh, P. Shekhar, D. Chakraborty, C. P. Vinod, R. Vaidhyanathan and E. Borguet, Synergistic electronic effects in AuCo nanoparticles stabilised in a triazine-based covalent organic framework: a catalyst for methyl orange

and methylene blue reduction, *ACS Appl. Nano Mater.*, 2022, **5**, 4744–4753.

52 L. Chen, L. Wang, Y. Wan, Y. Zhang, Z. Qi, X. Wu and H. Xu, Acetylene and Diacetylene Functionalized Covalent Triazine Frameworks as Metal-Free Photocatalysts for Hydrogen Peroxide Production: A New Two-Electron Water Oxidation Pathway, *Adv. Mater.*, 2020, **32**, 1904433.

53 F. Haase and B. V. Lotsch, Solving the COF trilemma: towards crystalline, stable and functional covalent organic frameworks, *Chem. Soc. Rev.*, 2020, **49**, 8469–8500.

54 A. Chakraborty, A. Alam, U. Pal, A. Sinha, S. Das, T. S. Dasgupta and P. Pachfule, Enhancing photocatalytic hydrogen peroxide generation by tuning hydrazone linkage density in covalent organic frameworks, *Nat. Commun.*, 2025, **16**, 503.

55 Z. Wang, J. Li, S. Liu, G. Shao and X. Zhao, A covalent organic framework/graphene aerogel electrocatalyst for enhanced overall water splitting, *Nanoscale*, 2022, **14**, 16944–16951.

56 X. Li, C. Zhang, S. Cai, X. Lei, V. Altoe, F. Hong, J. J. Urban, J. Ciston, E. M. Chan and Y. Liu, Facile transformation of imine covalent organic frameworks into ultrastable crystalline porous aromatic frameworks, *Nat. Commun.*, 2018, **9**, 2998.

57 C. J. Doonan, D. J. Tranchemontagne, T. G. Glover, J. R. Hunt and O. M. Yaghi, Exceptional ammonia uptake by a covalent organic framework, *Nat. Chem.*, 2010, **2**, 235–238.

58 H. Li, Q. Y. Pan, Y. C. Ma, X. Y. Guan, M. Xue, Q. R. Fang, Y. S. Yan, V. Valtchev and S. L. Qiu, Three-Dimensional Covalent Organic Frameworks with Dual Linkages for Bifunctional Cascade Catalysis, *J. Am. Chem. Soc.*, 2016, **138**, 14783–14788.

59 P. Rani, R. Das and C. M. Nagaraja, A review on framework (MOF/COF/POP)-based materials for efficient conversion of CO_2 to bio-active oxazolidinones, *Inorg. Chem. Front.*, 2025, **12**, 430–478.

60 H. Singh, V. K. Tomer, N. Jena, I. Bala, N. Sharma, D. Nepak, A. De Sarkar, K. Kailasam and S. K. Pal, A porous, crystalline truxene-based covalent organic framework and its application in humidity sensing, *J. Mater. Chem. A*, 2017, **5**, 21820–21827.

61 S. Ghosh, Y. Tsutsui, K. Suzuki, H. Kaji, K. Honjo, T. Uemura and S. Seki, Impact of the position of the imine linker on the optoelectronic performance of π-conjugated organic frameworks, *Mol. Syst. Des. Eng.*, 2019, **4**, 325–331.

62 S. Li, B. Kumbhakar, B. Mishra, J. Roeser, N. Chaoui, J. Schmidt, A. Thomas and P. Pachfule, Dithiophenedione-Based Covalent Organic Frameworks for Supercapacitive Energy Storage, *ACS Appl. Energy Mater.*, 2023, **6**, 9256–9263.

63 E. B. Agyekum, C. Nutakor, A. M. Agwa and S. Kamel, A Critical Review of Renewable Hydrogen Production Methods: Factors Affecting Their Scale-Up and Its Role in Future Energy Generation, *Membranes*, 2022, **12**, 173.

64 R. Das, P. K. Verma and C. M. Nagaraja, Design of Porphyrin-based Frameworks for Artificial Photosynthesis and Environmental Remediation: Recent Progress and Future Prospects, *Coord. Chem. Rev.*, 2024, **524**, 215944.

65 L. Stegbauer, K. Schwinghammer and B. V. Lotsch, A hydrazone-based covalent organic framework for photocatalytic hydrogen production, *Chem. Sci.*, 2014, **5**, 2789–2793.

66 B. Mishra, A. Alam, A. Chakraborty, B. Kumbhakar, S. Ghosh, P. Pachfule and A. Thomas, Covalent Organic Frameworks for Photocatalysis, *Adv. Mater.*, 2024, 2413118.

67 A. Nagar, G. Singh, A. Alam, P. Pachfule and C. M. Nagaraja, Benzothiadiazole-based Donor-Acceptor Covalent Organic Framework for Photocatalytic Hydrogen Generation, *Sustainable Energy Fuels*, 2025, **9**, 1885–1894.

68 S. Ghosh, A. Nakada, M. A. Springer, T. Kawaguchi, K. Suzuki, H. Kaji, I. Baburin, A. Kuc, T. Heine, H. Suzuki, R. Abe and S. Seki, Identification of Prime Factors to Maximize the Photocatalytic Hydrogen Evolution of Covalent Organic Frameworks, *J. Am. Chem. Soc.*, 2020, **142**, 9752–9762.

69 G. Zhang, M. Zhao, L. Su, H. Yu, C. Wang, D. Sun and Y. Ding, Donor-Acceptor Covalent-Organic Frameworks Based on Phthalimide as an Electron-Deficient Unit for Efficient Visible-Light Catalytic Hydrogen Evolution, *ACS Appl. Mater. Interfaces*, 2023, **15**, 20310–20316.

70 A. Ghosh, S. Menon, S. Biswas, S. Sahoo, A. Dey, R. Boomishankar, J. K. Zareba, U. V. Waghmare and T. K. Maji, Ferroelectric Dipolar Ordering in a Donor-Acceptor BasedCovalent-Organic Framework for Piezocatalytic WaterSplitting, *Adv. Funct. Mater.*, 2025, 2502787.

71 J. X. Koh, K. Geng and D. Jiang, Smart covalent organic frameworks: dual channel sensors for acids and bases, *Chem. Commun.*, 2021, **57**, 9418.

72 S. Yang, W. Liu, Y. Zhang, X. Jia, J. Sun, C. Zhang and M. Liu, A post-modified donor-acceptor covalent organic framework for enhanced photocatalytic H_2 production and high proton transport, *J. Mater. Chem. A*, 2024, **12**, 28161–28169.

73 Y. Li, L. Yang, H. He, L. Sun, H. Wang, X. Fang, Y. Zhao, D. Zheng, Y. Qi, Z. Li and W. Deng, In situ photodeposition of platinum clusters on a covalent organic framework for photocatalytic hydrogen production, *Nat. Commun.*, 2022, **13**, 1355.

74 E. Jin, Z. Lan, Q. Jiang, K. Geng, G. Li, X. Wang and D. Jiang, 2D sp^2 Carbon-Conjugated Covalent Organic Frameworks for Photocatalytic Hydrogen Production from Water, *Chemistry*, 2019, **5**, 1632–1647.